

CanonSLR: Canonical-View Guided Multi-View Continuous Sign Language Recognition

Xu Wang
wangxu2002@mail.hfut.edu.cn
Hefei University of Technology
Hefei, China

Shengeng Tang*
tangsg@hfut.edu.cn
Hefei University of Technology
Hefei, China

Wan Jiang
xjiangw000@gmail.com
Hefei University of Technology
Hefei, China

Yaxiong Wang
wangyx@hfut.edu.cn
Hefei University of Technology
Hefei, China

Lechao Cheng
chenglc@hfut.edu.cn
Hefei University of Technology
Hefei, China

Richang Hong
hongrc@hfut.edu.cn
Hefei University of Technology
Hefei, China

Abstract

Continuous Sign Language Recognition (CSLR) has achieved remarkable progress in recent years; however, most existing methods are developed under single-view settings and thus remain insufficiently robust to viewpoint variations in real-world scenarios. To address this limitation, we propose **CanonSLR**, a **canonical-view guided** framework for multi-view CSLR. Specifically, we introduce a frontal-view-anchored teacher-student learning strategy, in which a teacher network trained on frontal-view data provides canonical temporal supervision for a student network trained on all viewpoints. To further reduce cross-view semantic discrepancy, we propose Sequence-Level Soft-Target Distillation, which transfers structured temporal knowledge from the frontal view to non-frontal samples, thereby alleviating gloss boundary ambiguity and category confusion caused by occlusion and projection variation. In addition, we introduce Temporal Motion Relational Enhancement to explicitly model motion-aware temporal relations in high-level visual features, strengthening stable dynamic representations while suppressing viewpoint-sensitive appearance disturbances. To support multi-view CSLR research, we further develop a universal multi-view sign language data construction pipeline that transforms original single-view RGB videos into semantically consistent, temporally coherent, and viewpoint-controllable multi-view sign language videos. Based on this pipeline, we extend PHOENIX-2014T and CSL-Daily into two seven-view benchmarks, namely **PT14-MV** and **CSL-MV**, providing a new experimental foundation for multi-view CSLR. Extensive experiments on PT14-MV and CSL-MV demonstrate that CanonSLR consistently outperforms existing approaches under multi-view settings and exhibits stronger robustness, especially on challenging non-frontal views.

Keywords

Continuous Sign Language Recognition, Canonical-View Prior, Multi-view Learning

1 Introduction

Continuous Sign Language Recognition (CSLR) [10, 14, 18, 44] aims to automatically transcribe continuous sign language videos into gloss sequences, and is an important technique for improving communication accessibility between the deaf community and the

*Corresponding author.



Figure 1: Multi-view data curation across seven viewpoints: Front, R45°, R90°, L30°, L60°, U30°, and D30°.

broader information environment. Despite substantial progress on standard benchmarks [3, 20, 26, 50] driven by advances in visual representation learning [25, 31], sequence modeling [6, 9, 16], and large-scale pre-training [4, 17, 29], most existing CSLR systems are still developed and evaluated under a nearly fixed-view acquisition setting, where training and testing videos are captured from the same or very similar camera positions. As a result, their performance under current benchmarks may underestimate a practical yet underexplored challenge: *viewpoint robustness*.

This challenge is particularly critical for CSLR because sign language recognition depends heavily on fine-grained hand shapes, subtle local motions, and coordinated body-hand dynamics. Although viewpoint changes do not alter the underlying sign semantics, they can substantially perturb their visual manifestation, including hand appearance, motion projection, and occlusion patterns. Consequently, a model trained only under fixed-view settings may

rely on viewpoint-dependent visual shortcuts rather than stable semantic evidence. While recent studies improve CSLR through local region modeling [22, 52], skeletal priors [5, 47, 51] and contrastive learning [10, 49], they still largely assume single-view inputs. This mismatch between stable semantics and unstable visual evidence makes multi-view CSLR a fundamental problem for bringing sign language recognition closer to realistic deployment.

To address this issue, we propose **CanonSLR**, a **canonical-view guided** framework for multi-view CSLR based on teacher-student learning. Our key observation is that the main discrepancy across viewpoints lies not in sign semantics themselves, but in their viewpoint-dependent visual expressions. In existing CSLR data, the frontal view often provides the most informative and stable hand-body motion cues, and can therefore serve as a practical canonical semantic anchor. Based on this observation, we first train a teacher network using only frontal-view data, and then use it to guide a student network trained on data from all viewpoints. Specifically, we introduce **Sequence-level Soft-target Distillation (SSD)** to transfer canonical temporal semantics at the prediction level, thereby reducing gloss boundary ambiguity and category confusion caused by projection variation, occlusion, and local detail loss in non-frontal views. In addition, we propose **Temporal Motion Relational Enhancement (TME)** to strengthen motion-aware relational cues at the representation level, improving robustness to viewpoint-sensitive appearance changes. These two components operate at complementary levels: SSD aligns cross-view temporal predictions, while TME enhances view-invariant motion reasoning in intermediate features. A second obstacle is that current CSLR datasets do not provide a suitable benchmark foundation for systematically studying this problem. Mainstream datasets, such as PHOENIX-2014T [3] and CSL-Daily [50], as well as recently released in-the-wild sign language datasets [1, 13, 39, 41], are still predominantly built under single-view acquisition settings. Although a few recent efforts begin to explore multi-view sign language data construction [7, 28, 34], they mainly target isolated sign recognition and remain limited for continuous sign language scenarios. In practice, collecting real multi-view CSLR data is highly expensive, as it requires multi-camera deployment, viewpoint calibration, temporal synchronization, and cross-view annotation alignment.

To make multi-view CSLR studyable at scale, we further develop a **generic multi-view sign language data curation pipeline**. Given a single-view RGB video, the pipeline generates multi-view sign language videos that are semantically consistent, temporally coherent, and viewpoint-controllable through 3D human parameter estimation [2], root-driven viewpoint transformation, and skeleton-guided adaptive rendering [40, 48]. Based on this pipeline, as shown in Figure 1, we extend PHOENIX-2014T and CSL-Daily into seven-view training and evaluation benchmarks, denoted as **PT14-MV** and **CSL-MV**, respectively. These datasets provide a new and systematic experimental foundation for studying multi-view continuous sign language recognition.

Our contributions are summarized as follows:

- We propose **CanonSLR**, a canonical-view guided teacher-student framework for multi-view CSLR, which uses a frontal-view teacher to provide stable semantic supervision for non-frontal views.
- We introduce **Sequence-level Soft-target Distillation (SSD)** and **Temporal Motion Relational Enhancement (TME)** to improve cross-view temporal semantic transfer and strengthen motion-aware, viewpoint-robust representation learning.
- We develop a generic multi-view sign language data curation pipeline and build two seven-view CSLR benchmarks, **PT14-MV** and **CSL-MV**, establishing a new benchmark basis for multi-view continuous sign language recognition.

2 Related work

2.1 Continuous Sign Language Recognition

Continuous Sign Language Recognition aims to translate a continuous sequence of sign language video frames into its corresponding gloss sequence. Early CSLR approaches mainly relied on hand-crafted features [8, 15] and HMM-based temporal modeling [26, 27]. With the rise of deep learning, CNN- and RNN-based architectures have become the dominant paradigm for CSLR [14, 16, 25, 31]. A widely adopted framework typically consists of a visual feature extractor, usually a 2D or 3D CNN backbone, followed by a temporal modeling module such as an LSTM [36]. The introduction of the Connectionist Temporal Classification (CTC) loss [11] has further enabled end-to-end optimization without requiring precise frame-level gloss annotations [9, 18, 19].

Despite these advances, effectively learning discriminative visual representations for fine-grained hand dynamics remains a major challenge in CSLR. To address this issue, prior work has explored several directions. Some methods incorporate additional expert knowledge, such as skeletons [5, 47, 51], local regions [22, 52], or depth cues [21, 43], to guide feature learning, although such designs often increase computational overhead and model complexity. Other studies [6, 10, 16, 31] focus on stronger backbones, attention mechanisms, contrastive learning, and enhanced temporal modeling. Large-scale pre-training has also been explored to alleviate data scarcity and improve generalization [4, 29].

However, most existing CSLR methods are still developed under single-view assumptions. In real-world scenarios, viewpoint changes can alter hand appearance, motion projection, and occlusion patterns, making the same sign visually inconsistent across views. As a result, models trained under single-view settings often degrade markedly on unseen viewpoints. Therefore, a key yet underexplored challenge in CSLR is learning viewpoint-invariant semantics for robust multi-view recognition.

2.2 Sign Language Datasets

The performance of deep neural networks is highly dependent on large-scale and high-quality data, making dataset construction a fundamental topic in sign language research. For different sign language recognition tasks, a variety of benchmarks have been introduced to support algorithm development. In isolated sign language recognition (ISLR), datasets such as WLASL [28], MSASL [24], ASL [35], and MM-WLAuslan [34] have significantly advanced the field. For CSLR, PHOENIX-2014T [3] and CSL-Daily [50] have become the most widely used benchmarks. In addition, recent efforts have collected large-scale in-the-wild sign language corpora from the web, leading to thousand-hour datasets such as BoBSL [1], JWSign [13], YouTube-ASL [41], and YouTube-SL-25 [39].

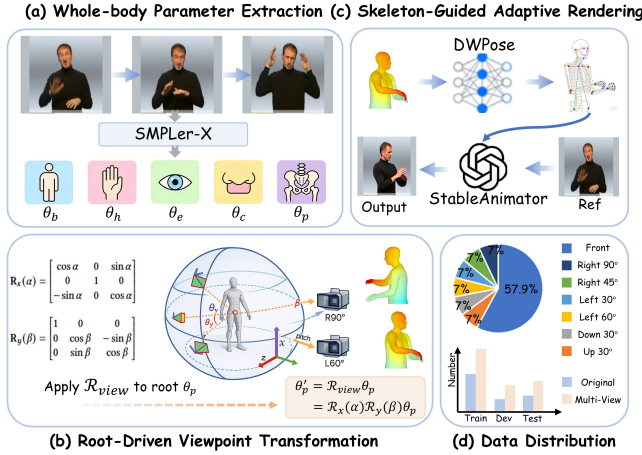


Figure 2: Multi-view data curation pipeline. (a) Whole-body parameter extraction. (b) Root-driven viewpoint transformation. (c) Skeleton-guided adaptive rendering. (d) View distribution of the constructed dataset.

However, despite the growing scale and diversity of existing datasets, most sign language benchmarks are still captured from a single, fixed viewpoint, making them inadequate for studying viewpoint robustness in CSLR. Although multi-view data have been explored in ISLR [7, 28, 34], they remain scarce for CSLR. Moreover, collecting real multi-view CSLR data is costly, as it requires multi-camera deployment, viewpoint calibration, temporal synchronization, and cross-view annotation alignment. Motivated by recent advances in 3D human parameter estimation, pose-driven modeling, and generative rendering, we instead construct semantically aligned multi-view data from single-view videos, providing a practical foundation for multi-view CSLR.

3 Multi-View Data Curation

Existing CSLR benchmarks are predominantly collected under single, fixed-view acquisition settings, which makes them inadequate for systematically studying viewpoint robustness or training multi-view CSLR models. To address this limitation, we orchestrate a multi-view sign language data construction pipeline that converts an original single-view sign video into multiple semantically consistent and viewpoint-controllable versions. As illustrated in Figure 2, the pipeline consists of three stages: *whole-body parameter extraction*, *root-driven viewpoint transformation*, and *skeleton-guided adaptive rendering*. Using this pipeline, we extend two widely used CSLR benchmarks, PHOENIX-2014T [3] and CSL-Daily [50], into their multi-view counterparts, denoted as **PT14-MV** and **CSL-MV**, respectively. The generated viewpoints include *Front*, *R45°*, *R90°*, *L30°*, *L60°*, *U30°*, and *D30°*, while preserving the original training/test splits and gloss annotations. A key requirement of this construction process is that the generated videos must remain semantically aligned with the original sign sequence. In our pipeline, viewpoint transformation changes only the visual observation of the same underlying motion trajectory, without altering the temporal order or linguistic content of the sign sequence. Therefore, the original gloss annotations can be directly inherited by all generated views.

3.1 Whole-body Parameter Extraction

Given an input single-view RGB video, we first recover a 3D parameterized whole-body representation for each frame using SMPLer-X [2], which is pre-trained on multiple human behavior datasets (e.g., 3DPW [42], COCO [23], InterHand2.6M [32], AGORA [33], and UBody [30]). The estimated pose parameters are denoted by

$$\theta_s = \{\theta_b, \theta_h, \theta_e, \theta_j, \theta_{root}\}, \quad (1)$$

where θ_b , θ_h , θ_e , θ_j , and θ_{root} represent the body pose, bilateral hand pose, eye pose, jaw pose, and global root orientation, respectively. The model also estimates body shape parameters β_s , facial expression parameters ψ , and camera parameters.

Based on these parameters, we reconstruct a 3D body mesh sequence together with the corresponding joint sequence. Compared with direct pixel-space manipulation, this parameterized 3D representation provides a more geometry-consistent basis for view synthesis and better preserves fine-grained sign-specific motion patterns under fast articulation, self-occlusion, and hand-body interaction.

3.2 Root-Driven Viewpoint Transformation

After recovering the 3D body representation, we synthesize new viewpoints by transforming the body in 3D space rather than manipulating images directly. We first remove the global translation and express the reconstructed body in a pelvis-centered coordinate system, so that viewpoint variation can be modeled as a global rigid rotation around the body root while preserving local pose configurations.

Let $\mathbf{V} \in \mathbb{R}^{M \times 3}$ denote the mesh vertices in the root-centered coordinate system, where M is the number of mesh vertices. Given a target viewpoint parameterized by yaw angle α and pitch angle β , the transformed mesh is defined as

$$\mathbf{V}' = \mathbf{R}_{view} \mathbf{V}, \quad \mathbf{R}_{view} = \mathbf{R}_y(\alpha) \mathbf{R}_x(\beta), \quad (2)$$

where

$$\mathbf{R}_y(\alpha) = \begin{bmatrix} \cos \alpha & 0 & \sin \alpha \\ 0 & 1 & 0 \\ -\sin \alpha & 0 & \cos \alpha \end{bmatrix}, \quad \mathbf{R}_x(\beta) = \begin{bmatrix} 1 & 0 & 0 \\ 0 & \cos \beta & -\sin \beta \\ 0 & \sin \beta & \cos \beta \end{bmatrix}. \quad (3)$$

The same transformation is applied consistently across all frames in the sequence. Since this operation only changes the observation angle of the recovered 3D motion, the relative temporal dynamics among the torso, arms, and hands are preserved by construction. This makes the transformed sequence semantically consistent with the original sign while avoiding the structural distortion and temporal artifacts that often arise in 2D warping or image-based view manipulation.

After rotation, we render the transformed mesh sequence with the corresponding target-view camera parameters to obtain an intermediate video V_{rot} . This intermediate result already preserves the correct coarse geometry and viewpoint change, but may still exhibit texture degradation or rendering artifacts, especially around the hands and face.

3.3 Skeleton-Guided Adaptive Rendering

To improve visual fidelity after viewpoint transformation, we perform a final skeleton-guided adaptive rendering stage. We first

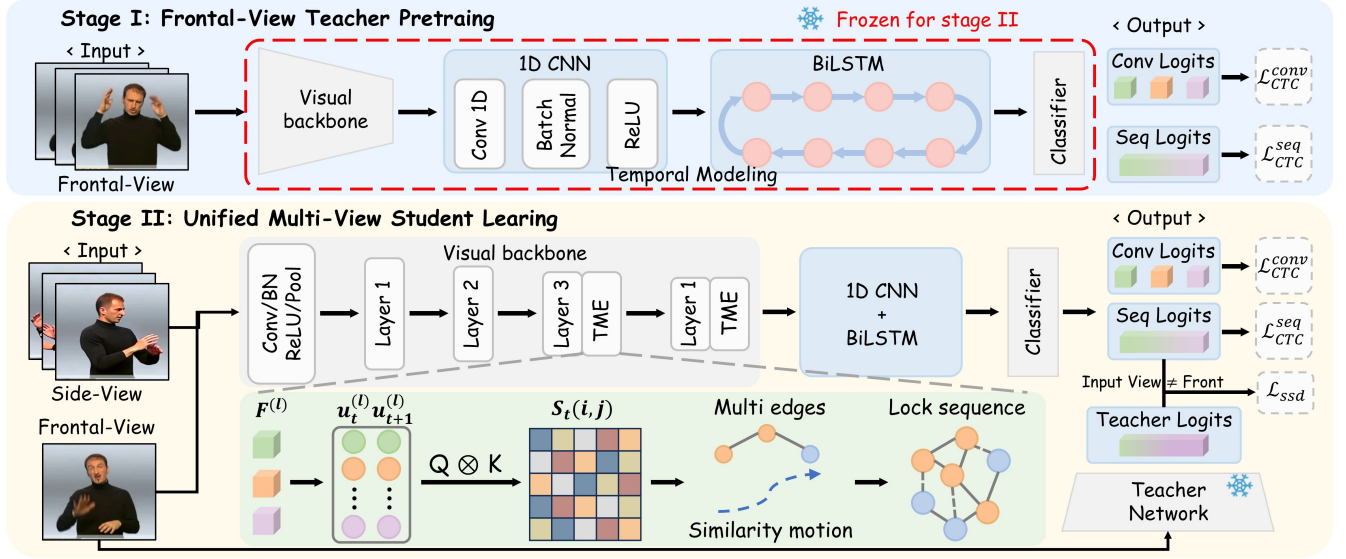


Figure 3: Overview of the proposed CanonSLR, a canonical-view guided framework for multi-view CSLR. In Stage I, a frontal-view teacher network is pretrained to learn canonical temporal semantics. In Stage II, the teacher is frozen to supervise a unified multi-view student trained on all viewpoints. SSD transfers canonical temporal knowledge from the frontal view to non-frontal samples, while TME strengthens motion-aware feature learning to improve robustness against viewpoint variations.

apply DWPose [48] to the intermediate video V_{rot} to extract a temporally consistent 2D skeleton sequence, which serves as explicit motion guidance for subsequent rendering. The extracted skeleton is then fed into StableAnimator [40] together with identity cues from the original video, enabling the model to synthesize a realistic target-view video V_{final} .

This stage is particularly important for CSLR because sign semantics depend strongly on subtle hand articulation, local contour details, and temporally coherent motion. Skeleton guidance helps preserve motion structure under viewpoint change, while identity conditioning maintains signer appearance and reduces semantic drift during rendering. In addition, the adversarial training strategy and optical-flow consistency constraints in StableAnimator help improve temporal smoothness and local visual realism, especially for hand regions and rapid motion transitions.

Through the above three stages, the proposed pipeline transforms a single-view CSLR video into multiple new views while maintaining semantic consistency, temporal coherence, and realistic appearance. Based on this process, we construct two seven-view benchmarks, **PT14-MV** and **CSL-MV**, which provide a systematic data foundation for multi-view CSLR.

4 Method

4.1 Overall Framework

Given a multi-view training set $\mathcal{D} = \{(X_n^v, Y_n)\}_{n=1}^N$, where X_n^v denotes the sign video of the n -th sample captured under viewpoint v and Y_n denotes its gloss sequence, our goal is to learn a unified CSLR model that remains robust to viewpoint variation. As illustrated in Figure 3, the proposed **CanonSLR** is organized as a two-stage training framework.

Stage I: Frontal-View Teacher Pretraining. (cf. section 4.2) In the first stage, we train a teacher network using only frontal-view

data. Since the frontal view typically provides the most complete and stable hand-body motion cues, this stage aims to learn canonical temporal semantics under the anchor view. The pretrained teacher is then frozen and used as a stable semantic reference for subsequent cross-view learning.

Stage II: Unified Multi-View Student Learning. (cf. section 4.3)

In the second stage, a unified student network is trained on videos from all viewpoints under the guidance of the frozen teacher. This stage is built upon two complementary mechanisms. First, **Sequence-Level Soft-Target Distillation (SSD)** transfers canonical temporal semantics from the frontal-view teacher to non-frontal samples, thereby reducing cross-view semantic discrepancy at the prediction level. Second, **Temporal Motion Relational Enhancement (TME)** is incorporated into the student backbone to strengthen motion-aware relational modeling and suppress viewpoint-sensitive appearance disturbance at the representation level. Through these two mechanisms, the student progressively acquires both canonical temporal supervision and view-robust motion representations.

During inference, only the student network is retained, enabling efficient multi-view CSLR without introducing additional teacher-side computational overhead.

4.2 Frontal-View-Anchored Teacher Network

To establish a canonical semantic anchor for cross-view learning, we first train a teacher network using only frontal-view sign videos. Given a frontal-view input sequence

$$X^f = \{x_t^f\}_{t=1}^T \in \mathbb{R}^{T \times 3 \times H \times W}, \quad (4)$$

the teacher aims to predict the corresponding gloss sequence

$$Y = \{y_m\}_{m=1}^M, \quad (5)$$

where T and M denote the video length and gloss sequence length, respectively.

The input video is first processed by a ResNet-18 visual encoder to extract frame-wise visual features:

$$V^{\text{tea}} = \text{ResNet}(X^f), \quad (6)$$

where $V^{\text{tea}} = \{v_t^{\text{tea}}\}_{t=1}^T$ denotes the resulting temporal feature sequence. These features are then passed to a temporal modeling module consisting of a 1D CNN and a BiLSTM, which capture short-range temporal dynamics and long-range temporal dependencies, respectively:

$$\tilde{H}^{\text{tea}} = \text{CNN}(V^{\text{tea}}), \quad H^{\text{tea}} = \text{BiLSTM}(\tilde{H}^{\text{tea}}). \quad (7)$$

A gloss classification head further projects the temporal representation into the gloss space:

$$Z^{\text{tea}} = \text{Classifier}(H^{\text{tea}}), \quad (8)$$

where Z^{tea} denotes the teacher's temporal gloss logits. Since the teacher is optimized only on frontal-view samples, it captures canonical temporal semantics without being affected by cross-view appearance variation. During student training, the teacher is frozen and used as a stable semantic reference for subsequent cross-view knowledge transfer.

4.3 Unified Multi-View Student Network

After obtaining the frontal-view teacher in Stage I, we freeze all teacher parameters and train a unified student network on data from all viewpoints. The goal of this stage is to learn a single CSLR model that remains robust under viewpoint variation while preserving stable temporal semantics. To this end, Stage II combines three elements within one unified training framework: (i) a multi-view student recognizer, (ii) **Temporal Motion Relational Enhancement (TME)** for motion-aware feature learning, and (iii) **Sequence-Level Soft-Target Distillation (SSD)** for cross-view semantic transfer from the frozen teacher.

Student network. The student network \mathcal{F}_{stu} is the final model used for multi-view recognition. It follows the same overall architecture as the teacher, including a ResNet-based visual backbone, a temporal modeling module, and a gloss classification head. Given an input video X^v captured under viewpoint v , the student produces both auxiliary convolutional logits and final sequence logits:

$$\tilde{Z}^{\text{stu}}, Z^{\text{stu}} = \mathcal{F}_{\text{stu}}(X^v), \quad (9)$$

where \tilde{Z}^{stu} denotes the auxiliary logits from the convolutional temporal branch and Z^{stu} denotes the final sequence logits.

Since the student is trained on videos from all viewpoints, it must learn to reduce viewpoint-sensitive appearance variation while preserving viewpoint-invariant sign semantics. For gloss supervision, we adopt the standard CTC objective [11]:

$$\mathcal{L}_{\text{CTC}} = -\log p(Y | X; \theta) = -\log \sum_{\pi \in \mathcal{B}^{-1}(Y)} p(\pi | X; \theta), \quad (10)$$

where Y denotes the target gloss sequence, π is a valid alignment path, and $\mathcal{B}(\cdot)$ denotes the CTC collapsing operator. Accordingly, two CTC losses are imposed on the student outputs:

$$\mathcal{L}_{\text{CTC}}^{\text{stu}} = \mathcal{L}_{\text{CTC}}^{\text{conv}}(\tilde{Z}^{\text{stu}}, Y) + \mathcal{L}_{\text{CTC}}^{\text{seq}}(Z^{\text{stu}}, Y). \quad (11)$$

Temporal Motion Relational Enhancement. To improve viewpoint robustness at the representation level, we augment the student backbone with **Temporal Motion Relational Enhancement**

(**TME**). The key motivation is that viewpoint changes mainly perturb local appearance and spatial projection, whereas more stable discriminative cues are often encoded in temporal motion dynamics and their relational structure across adjacent frames.

Let $\mathbf{F}^{(l)} \in \mathbb{R}^{C_l \times T \times H_l \times W_l}$ denote the intermediate feature tensor at the l -th high-level stage of the student ResNet backbone, where the batch dimension is omitted for simplicity. TME first reshapes the feature map at each time step into a set of spatial tokens:

$$\mathbf{U}_t^{(l)} = \text{Reshape}(\mathbf{F}_{:,t,:,:}^{(l)}) \in \mathbb{R}^{B_l \times C_l}, \quad B_l = H_l \times W_l, \quad (12)$$

and the token sequence is written as $\mathbf{U}^{(l)} = \{\mathbf{U}_t^{(l)}\}_{t=1}^T$.

To capture motion correspondences between adjacent frames, the tokens from frames t and $t+1$ are projected into a shared query-key space:

$$\mathbf{Q}_t^{(l)} = \mathbf{U}_t^{(l)} \mathbf{W}_q^{(l)}, \quad \mathbf{K}_{t+1}^{(l)} = \mathbf{U}_{t+1}^{(l)} \mathbf{W}_k^{(l)}, \quad (13)$$

where $\mathbf{W}_q^{(l)}, \mathbf{W}_k^{(l)} \in \mathbb{R}^{C_l \times d}$ are learnable projection matrices. The correlation between the i -th token in frame t and the j -th token in frame $t+1$ is then computed as

$$S_t^{(l)}(i, j) = \frac{(\mathbf{q}_{t,i}^{(l)})^\top \mathbf{k}_{t+1,j}^{(l)}}{\sqrt{d}}, \quad t = 1, \dots, T-1. \quad (14)$$

Based on $S_t^{(l)}$, we retain, for each token in frame t , the top- K most correlated tokens in frame $t+1$ to construct a sparse temporal graph:

$$\mathcal{E}_t^{(l)} = \left\{ (v_{t,i}, v_{t+1,j}) \mid j \in \text{TopK}(S_t^{(l)}(i, :)) \right\}, \quad \mathcal{E}^{(l)} = \bigcup_{t=1}^{T-1} \mathcal{E}_t^{(l)}. \quad (15)$$

All sequence tokens are then concatenated as graph nodes:

$$\mathbf{G}^{(l)} \in \mathbb{R}^{(T \cdot B_l) \times C_l}. \quad (16)$$

A graph convolution network is applied over the resulting sparse graph to aggregate motion-consistent information:

$$\mathbf{X}_{\text{gcn}}^{(l)} = \text{GCN}(\mathbf{G}^{(l)}, \mathcal{E}^{(l)}). \quad (17)$$

The enhanced feature is finally reshaped back to the original layout and residually fused with the backbone feature:

$$\mathcal{T}^{(l)}(\mathbf{F}^{(l)}) = \text{Reshape}(\mathbf{X}_{\text{gcn}}^{(l)}), \quad \hat{\mathbf{F}}^{(l)} = \mathbf{F}^{(l)} + \alpha_l \mathcal{T}^{(l)}(\mathbf{F}^{(l)}), \quad (18)$$

where α_l is a learnable scalar. In practice, TME is inserted into the student ResNet-18 backbone after the third and fourth residual stages. By explicitly modeling motion correspondences across adjacent frames, TME enhances motion-aware visual features before temporal modeling and suppresses viewpoint-sensitive appearance disturbance.

Sequence-Level Soft-Target Distillation. Although the student is trained on all viewpoints, directly optimizing it with hard gloss labels alone may still lead to severe semantic discrepancy across views. To alleviate this issue, we introduce **Sequence-Level Soft-Target Distillation (SSD)** from the frozen frontal-view teacher.

Specifically, for each non-frontal sample, the student is supervised not only by the ground-truth gloss sequence, but also by the teacher's soft temporal outputs. Since the teacher and student may produce logits with different temporal lengths after temporal modeling, we first align the teacher logits to the temporal resolution of

Table 1: Comparison with state-of-the-art methods for CSLR on the PT14-MV and CSL-MV datasets.

Methods	Venue	PT14-MV				CSL-MV			
		Dev-WER↓	Dev-del↓/ins↓	Test-WER↓	Test-del↓/ins↓	Dev-WER↓	Dev-del↓/ins↓	Test-WER↓	Test-del↓/ins↓
SMKD [16]	ICCV 2021	42.83	17.61/2.06	42.91	16.06/2.68	45.78	16.56/2.23	45.01	16.24/2.24
VAC [31]	ICCV 2021	39.85	16.20/2.35	39.57	16.21/3.21	46.62	18.31/2.41	44.59	17.15/2.46
MMTLB [4]	CVPR 2022	38.89	12.88/4.33	38.05	11.55/4.57	44.28	16.44/3.71	43.28	15.02/3.74
C ² SLR [52]	CVPR 2022	41.90	19.10/2.40	40.50	18.50/2.9	46.64	18.31/1.96	45.22	18.08/1.89
SEN [19]	AAAI 2023	37.77	14.77/2.61	38.17	14.18/3.34	42.23	13.08/3.36	41.11	12.25/3.31
CorrNet [18]	CVPR 2023	34.93	12.50/2.36	34.80	11.61/2.95	41.21	13.47/3.41	40.21	12.54/2.95
SignGraph [9]	CVPR 2024	34.65	11.58/2.65	35.13	10.52/3.53	38.63	13.50/2.93	37.63	12.79/2.59
HSTE [46]	ICASSP 2025	42.03	17.21/2.11	40.31	18.23/2.95	44.33	16.32/3.73	42.74	14.23/3.55
MSKA [12]	PR 2025	45.25	-	45.45	-	48.09	-	47.39	-
Ours	-	33.22	13.39/2.15	33.43	12.05/2.89	37.72	14.57/2.52	36.60	13.65/2.50

Table 2: Details of new datasets.

Datasets	Train	Dev	Test	Total
PT14	7096	519	642	8257
PT14-MV	11896 ^{↑4800}	1119 ^{↑600}	1242 ^{↑600}	14257 ^{↑6000}
CSL	18401	1077	1176	20654
CSL-MV	23201 ^{↑4800}	1677 ^{↑600}	1776 ^{↑600}	26654 ^{↑6000}

the student via interpolation, and denote the aligned logits by \tilde{Z}^{tea} . We then define the distillation loss as

$$\mathcal{L}_{\text{SSD}} = \mathbb{I}[v \neq f] \cdot T_d^2 D_{\text{KL}} \left(\sigma \left(\frac{\tilde{Z}^{\text{tea}}}{T_d} \right) \parallel \sigma \left(\frac{Z^{\text{stu}}}{T_d} \right) \right), \quad (19)$$

where $\mathbb{I}[v \neq f]$ is an indicator function that activates distillation only for non-frontal samples, f denotes the frontal view, $D_{\text{KL}}(\cdot \parallel \cdot)$ denotes Kullback–Leibler divergence, $\sigma(\cdot)$ denotes the softmax function, and T_d is the distillation temperature.

This design allows the student to inherit smoother and more structured temporal decision boundaries from the canonical-view teacher, thereby alleviating gloss ambiguity and category confusion caused by projection variation, self-occlusion, and local detail loss in non-frontal views.

Training objective. The overall optimization objective of Stage II is given by

$$\mathcal{L}_{\text{stu}} = \mathcal{L}_{\text{CTC}}^{\text{conv}}(\tilde{Z}^{\text{stu}}, Y) + \mathcal{L}_{\text{CTC}}^{\text{seq}}(Z^{\text{stu}}, Y) + \lambda_{\text{SSD}} \mathcal{L}_{\text{SSD}}, \quad (20)$$

where λ_{SSD} is the loss weight for distillation.

Through this unified Stage II learning process, the student simultaneously acquires canonical temporal supervision from the frontal-view teacher and motion-aware view-robust representations from TME. During inference, only the student network is retained, enabling efficient multi-view CSLR without introducing any additional teacher-side overhead.

5 Experiments

5.1 Experimental Settings

Datasets. All experiments are conducted on two newly constructed multi-view CSLR benchmarks, **PT14-MV** and **CSL-MV**, which are built upon Phoenix-2014T [3] and CSL-Daily [50], respectively. Each benchmark contains seven viewpoints, namely *Front*, *L30°*,

L60°, *R45°*, *R90°*, *U30°*, and *D30°*. To ensure balanced view construction while avoiding overlap across data splits, we sample 800, 100, and 100 source instances from the original train, dev and test sets, respectively, and generate their corresponding multi-view versions. The resulting datasets serve as the primary evaluation benchmarks for multi-view CSLR. Detailed statistics are reported in Table 2.

Evaluation Metric. Following prior CSLR works [4, 9, 37, 38, 45, 52], we use Word Error Rate (WER) as the evaluation metric:

$$\text{WER} = \frac{\#\text{sub} + \#\text{ins} + \#\text{del}}{\#\text{ref}}, \quad (21)$$

where $\#\text{sub}$, $\#\text{ins}$ and $\#\text{del}$ denote the numbers of substitutions, insertions and deletions required to transform the predicted gloss sequence into the reference sequence. $\#\text{ref}$ denotes the number of glosses in the reference. Lower WER indicates better performance.

Implementation Details. We adopt a ResNet-18 visual backbone for both the teacher and student networks, and use the same temporal modeling architecture in both stages. In Stage I, the frontal-view teacher is trained for 40 epochs using Adam with an initial learning rate of 1×10^{-4} . In Stage II, the teacher is frozen and the student is trained on the full multi-view dataset using convolution-level CTC loss, sequence-level CTC loss, and the proposed distillation loss. The distillation temperature is set to $T_d = 8$, and the distillation loss weight is set to $\lambda_{\text{SSD}} = 40.0$. Training is implemented with PyTorch Distributed Data Parallel and a MultiStep learning rate decay schedule. During decoding, we use beam search to compute WER. All experiments are conducted on 8 NVIDIA RTX 4080S GPUs.

5.2 Comparison with State-of-the-Art Methods

Table 1 reports the comparison with representative state-of-the-art continuous sign language recognition methods on the proposed PT14-MV and CSL-MV benchmarks. For fair comparison, all competing methods are retrained on these two multi-view datasets following the training protocols and implementation details described in their original papers. As shown, **CanonSLR** achieves the best performance on all evaluation splits of both datasets. On **PT14-MV**, CanonSLR obtains **33.22%** WER on the dev set and **33.43%** on the test set, improving over the strongest baseline by **1.43** and **1.37** absolute WER points, respectively. On **CSL-MV**, it further achieves **37.72%** and **36.60%** WER on the dev and test sets, surpassing the

Table 3: Ablation results of different module combinations on the PT14-MV dataset. “ALL” represents all data; “R”, “L”, “D”, and “U” represent right rotation, left rotation, downward tilt and upward tilt, respectively. Δ indicates the performance change compared with the Baseline. Lower WER indicates better performance.

Methods			Multi-view		Large angle			Small angle			Pitch			Front	
Baseline	SSD	TME	All	Δ	R90°	L60°	Δ_{Avg}	R45°	L30°	Δ_{Avg}	D30°	U30°	Δ_{Avg}	0°	Δ
✓			37.73	-	58.04	50.73	-	53.91	52.52	-	55.05	52.10	-	22.99	-
✓	✓		35.93	↓1.80	55.20	46.41	↓3.58	49.92	51.42	↓2.55	48.50	47.83	↓5.41	23.08	↑0.09
✓		✓	34.51	↓3.22	55.74	45.89	↓3.57	47.93	46.85	↓5.83	44.65	46.50	↓8.00	22.14	↓0.85
✓	✓	✓	33.43	↓4.30	53.21	43.05	↓6.26	46.55	46.23	↓6.83	42.49	44.88	↓9.89	21.79	↓1.20

best competing results by **0.91** and **1.03** absolute WER points, respectively. These consistent gains across both benchmarks indicate that CanonSLR effectively reduces cross-view semantic discrepancy and learns more robust viewpoint-invariant representations under multi-view CSLR settings.

5.3 Ablation Study

Effectiveness of the SSD and TME. We evaluate the individual contributions of the proposed modules on **PT14-MV** across different viewpoints, as summarized in Table 3. Here, “Avg” denotes the mean WER of two views in each category, and Δ_{Avg} denotes the improvement relative to the baseline. The baseline model degrades significantly under large viewpoint variations, particularly for pitch views (D30°, U30°) and extreme horizontal angles (R90°, L60°). Introducing **SSD** reduces the overall WER by **1.80** points, with larger gains on challenging views, including **3.58** points for large-angle views and **5.41** points for pitch views. This indicates that canonical-view supervision effectively alleviates projection-induced semantic ambiguity. Applying **TME** alone yields a larger overall improvement of **3.22** points. Unlike SSD, which focuses on prediction-level alignment, TME consistently improves performance across all viewpoints, including a **0.85**-point gain on the frontal view and an **8.00**-point gain on pitch views. This demonstrates its effectiveness in learning motion-aware, view-invariant representations. Combining both modules achieves the best performance with an overall WER of **33.43%**. The improvement is especially pronounced under extreme viewpoint changes, where pitch views achieve a **9.89**-point reduction. These results indicate that SSD and TME are complementary, addressing cross-view discrepancy at the semantic and representation levels, respectively.

Mid-to-high layers are optimal for TME. We analyze the impact of inserting TME at different backbone stages, as shown in Fig. 4(a). The layer1 setting is omitted due to prohibitive memory cost. Among single-layer configurations, layer3 achieves the best performance, indicating that mid-to-high-level features are more suitable for modeling stable temporal relations. Extending TME to layer3+4 further improves side-view performance, suggesting that motion representations from layer3 and semantic representations from layer4 are complementary. Considering both performance and computational cost, we adopt layer3+4 in the final model.

Moderate λ gives the best trade-off. To evaluate the robustness of the proposed SSD, we conduct a sensitivity analysis on the loss weight parameter λ , which controls the balance between the primary CTC objective and the teacher’s supervision. As illustrated

in Figure 4(b), we vary λ across the range of {5, 10, 20, 40, 80} and monitor the WER on both the dev and test sets. The dev curve exhibits a relatively stable descent, reaching its optimal performance of 33.22% at $\lambda = 40$. Beyond $\lambda = 80$, the performance slightly degrades, suggesting that an excessively large distillation weight may overwhelm the hard-label CTC constraints and cause the model to overfit the teacher’s soft distribution. While the test set demonstrates more fluctuation—a common phenomenon in CSLR tasks under complex multi-view settings—it perfectly aligns with the dev set at the optimal threshold, yielding the lowest test WER of 33.43% at $\lambda = 40$. Consequently, we set $\lambda = 40$ as the default configuration, ensuring an optimal equilibrium between task-specific learning and cross-view semantic transfer.

Canonical-view guidance improves optimization. To verify the effectiveness of canonical-view prior guidance, we compare the training process with and without canonical-view guidance. As shown in Figure 4(c), canonical-view guidance not only converges faster, reaching the same WER level at an earlier stage, but also maintains consistently lower error rates throughout training. This indicates that the canonical-view provides more stable and effective supervision, improving both optimization efficiency and final recognition performance.

The frontal view is the most effective canonical anchor. We further analyze which view is the most suitable choice as the canonical anchor by evaluating four candidates, namely *Front*, *L60°*, *R30°*, and *D30°*. The results are summarized in Figure 4(d), where we report the WER on the **All**, the average WER over **All side-view**, and the **Front** subset. Among all candidates, using the frontal view as the canonical anchor yields the best overall performance, achieving the lowest WER of 33.43% on All and 46.07% on All side-view. Although the *L60°* anchor obtains a slightly lower WER on the frontal subset, its overall and side-view performance degrades noticeably. The *R30°* and *D30°* anchors show a similar trend, producing consistently higher WER on both the All set and the side-view evaluation. These results suggest that the frontal view serves as the most effective canonical anchor, as it provides the most complete and stable visual cues for guiding the student network and promotes stronger cross-view semantic transfer.

5.4 Qualitative Visualization Analysis

Visualization of Data Quality and Viewpoint Challenges As shown in Figure 5, we visualize the same sign sample after viewpoint transformation under different viewpoints. The generated

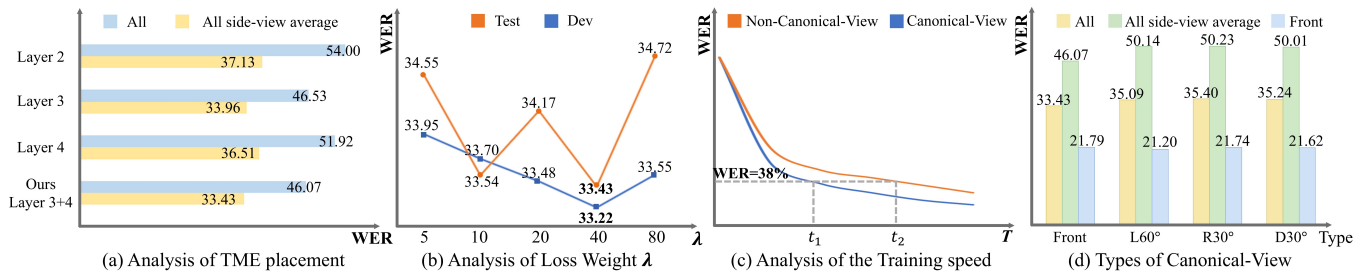


Figure 4: Detailed analysis of the designed CanonSLR on the PT14-MV dataset, where (a), (c), (d) report the performance on the test set. (a) Hierarchical Placement Analysis of the TME Module. (b) Sensitivity analysis of the distillation weight λ . (c) Comparison of canonical-view and non-canonical-view guidance. (d) Comparison of different canonical-view anchors.

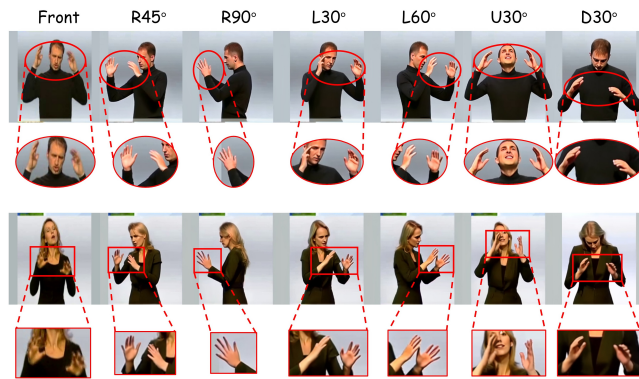


Figure 5: Visualization of the same sign sample under multiple viewpoints with evident appearance variations.

samples preserve good semantic consistency and temporal coherence across views, while the body structure, hand motions, and critical local details are well retained, demonstrating the high quality and usability of the constructed data. Meanwhile, viewpoint changes still cause obvious variations in body contour, relative hand positions, and fine-grained hand-shape details, especially under side and pitch views where occlusion and projection distortion become more severe. This indicates that the challenge of multi-view CSLR lies not in semantic changes themselves, but in the inconsistency of visual manifestations across viewpoints, and further shows that multi-view sign language understanding is more challenging than the conventional single-view setting.

Visualization of Recognition Results As shown in Figure 6, we further present a qualitative comparison of different methods. Under challenging viewpoint conditions, existing methods are more prone to semantic confusion and missing glosses. For example, in case (a), CorrNet misrecognizes “KOENNEN” as “MOEGLICH”, while SEN further confuses “WEST” with “SUEDWEST”; in case (b), both CorrNet and SEN produce more obvious word substitution and semantic deviation errors. In contrast, our method correctly recovers the complete gloss sequences, demonstrating stronger robustness under multi-view settings. This indicates that the proposed teacher-student learning strategy effectively alleviates cross-view semantic discrepancy, while TME further improves the modeling of stable motion cues.



Figure 6: Qualitative comparison of different methods on multi-view CSLR. Red words indicate incorrect predictions, while blue words denote missing glosses.

6 Conclusions

In this paper, we presented **CanonSLR**, a **canonical-view guided** framework for multi-view continuous sign language recognition. The core idea of CanonSLR is to treat the frontal view as a canonical semantic anchor, and use it to guide the learning of a unified recognizer across diverse viewpoints. Based on this insight, we introduced a frontal-view-anchored teacher-student learning strategy, where the teacher provides canonical temporal supervision for the student under multi-view settings. We further proposed Sequence-Level Soft-Target Distillation to transfer canonical temporal knowledge from frontal to non-frontal views, and Temporal Motion Relational Enhancement to strengthen motion-aware and view-robust feature learning. In addition, to support multi-view CSLR research, we developed a universal multi-view sign language data construction pipeline and extended PHOENIX-2014T and CSL-Daily into two seven-view benchmarks, PT14-MV and CSL-MV. Extensive experiments demonstrate that CanonSLR consistently outperforms existing methods, especially under challenging non-frontal views. These results verify the effectiveness of canonical-view guidance for reducing cross-view semantic discrepancy and highlight its potential for advancing robust real-world CSLR.

References

- [1] Samuel Albanie, Gül Varol, Liliane Momeni, Hannah Bull, Triantafyllos Afouras, Himel Chowdhury, Neil Fox, Bencie Woll, Rob Cooper, Andrew McParland, et al. 2021. Bbc-oxford british sign language dataset. *arXiv preprint arXiv:2111.03635* (2021).
- [2] Zhongang Cai, Wanqi Yin, Ailing Zeng, Chen Wei, Qingping Sun, Wang Yanjun, Hui En Pang, Haiyi Mei, Mingyuan Zhang, Lei Zhang, et al. 2023. Smpler-x: Scaling up expressive human pose and shape estimation. *Neural Information Processing Systems* 36 (2023), 11454–11468.
- [3] Necati Cihan Camgoz, Simon Hadfield, Oscar Koller, Hermann Ney, and Richard Bowden. 2018. Neural sign language translation. In *Proceedings of the IEEE conference on computer vision and pattern recognition*. 7784–7793.
- [4] Yutong Chen, Fangyun Wei, Xiao Sun, Zhirong Wu, and Stephen Lin. 2022. A simple multi-modality transfer learning baseline for sign language translation. In *Proceedings of the IEEE/CVF conference on computer vision and pattern recognition*. 5120–5130.
- [5] Yutong Chen, Ronglai Zuo, Fangyun Wei, Yu Wu, Shujie Liu, and Brian Mak. 2022. Two-stream network for sign language recognition and translation. *Advances in Neural Information Processing Systems* 35 (2022), 17043–17056.
- [6] Ka Leong Cheng, Zhaoyang Yang, Qifeng Chen, and Yu-Wing Tai. 2020. Fully convolutional networks for continuous sign language recognition. In *European Conference on Computer Vision*. Springer, 697–714.
- [7] Aashaka Desai, Lauren Berger, Fyodor Minakov, Nessa Milano, Chinmay Singh, Kriston Pumphrey, Richard Ladner, Hal Daumé III, Alex X Lu, Naomi Caselli, et al. 2023. ASL citizen: a community-sourced dataset for advancing isolated sign language recognition. *Advances in Neural Information Processing Systems* 36 (2023), 76893–76907.
- [8] William T Freeman and Michal Roth. 1995. Orientation histograms for hand gesture recognition. In *International workshop on automatic face and gesture recognition*, Vol. 12. Zurich, Switzerland, 296–301.
- [9] Shiwei Gan, Yafeng Yin, Zhiwei Jiang, Hongkai Wen, Lei Xie, and Sanglu Lu. 2024. Signgraph: A sign sequence is worth graphs of nodes. In *Proceedings of the IEEE/CVF Conference on Computer Vision and Pattern Recognition*. 13470–13479.
- [10] Shiwei Gan, Yafeng Yin, Zhiwei Jiang, Kang Xia, Lei Xie, and Sanglu Lu. 2023. Contrastive Learning for Sign Language Recognition and Translation.. In *IJCAI* 763–772.
- [11] Alex Graves, Santiago Fernández, Faustino Gomez, and Jürgen Schmidhuber. 2006. Connectionist temporal classification: labelling unsegmented sequence data with recurrent neural networks. In *Proceedings of the 23rd international conference on Machine learning*. 369–376.
- [12] Mo Guan, Yan Wang, Guangkun Ma, Jiarui Liu, and Mingzu Sun. 2025. MSKA: Multi-stream keypoint attention network for sign language recognition and translation. *Pattern Recognition* 165 (2025), 111602.
- [13] Shester Gueuwou, Sophie Siake, Colin Leong, and Mathias Müller. 2023. JWSign: A highly multilingual corpus of Bible translations for more diversity in sign language processing. *arXiv preprint arXiv:2311.10174* (2023).
- [14] Dan Guo, Shengeng Tang, and Meng Wang. 2019. Connectionist Temporal Modeling of Video and Language: A Joint Model for Translation and Sign Labeling. In *International Joint Conference on Artificial Intelligence*. 751–757.
- [15] Junwei Han, George Awad, and Alistair Sutherland. 2009. Modelling and segmenting subunits for sign language recognition based on hand motion analysis. *Pattern recognition letters* 30, 6 (2009), 623–633.
- [16] Aiming Hao, Yuecong Min, and Xilin Chen. 2021. Self-mutual distillation learning for continuous sign language recognition. In *Proceedings of the IEEE/CVF international conference on computer vision*. 11303–11312.
- [17] Hezhen Hu, Weichao Zhao, Wengang Zhou, and Houqiang Li. 2023. Signbert+: Hand-model-aware self-supervised pre-training for sign language understanding. *IEEE Transactions on Pattern Analysis and Machine Intelligence* 45, 9 (2023), 11221–11239.
- [18] Lianyu Hu, Liqing Gao, Zekang Liu, and Wei Feng. 2023. Continuous sign language recognition with correlation network. In *Proceedings of the IEEE/CVF Conference on Computer Vision and Pattern Recognition*. 2529–2539.
- [19] Lianyu Hu, Liqing Gao, Zekang Liu, and Wei Feng. 2023. Self-emphasizing network for continuous sign language recognition. In *Proceedings of the AAAI conference on artificial intelligence*, Vol. 37. 854–862.
- [20] Jie Huang, Wengang Zhou, Qilin Zhang, Houqiang Li, and Weiping Li. 2018. Video-based sign language recognition without temporal segmentation. In *Proceedings of the AAAI conference on artificial intelligence*, Vol. 32.
- [21] Songyao Jiang, Bin Sun, Lichen Wang, Yue Bai, Kumpeng Li, and Yun Fu. 2021. Skeleton aware multi-modal sign language recognition. In *Proceedings of the IEEE/CVF conference on computer vision and pattern recognition*. 3413–3423.
- [22] Peiqi Jiao, Yuecong Min, Yanan Li, Xiaotao Wang, Lei Lei, and Xilin Chen. 2023. Cosign: Exploring co-occurrence signals in skeleton-based continuous sign language recognition. In *Proceedings of the IEEE/CVF international conference on computer vision*. 20676–20686.
- [23] Sheng Jin, Lumin Xu, Jin Xu, Can Wang, Wentao Liu, Chen Qian, Wanli Ouyang, and Ping Luo. 2020. Whole-body human pose estimation in the wild. In *European Conference on Computer Vision*. Springer, 196–214.
- [24] Hamid Reza Vaezi Joze and Oscar Koller. 2018. Ms-asl: A large-scale data set and benchmark for understanding american sign language. *arXiv preprint arXiv:1812.01053* (2018).
- [25] Oscar Koller, Necati Cihan Camgoz, Hermann Ney, and Richard Bowden. 2019. Weakly supervised learning with multi-stream CNN-LSTM-HMMs to discover sequential parallelism in sign language videos. *IEEE transactions on pattern analysis and machine intelligence* 42, 9 (2019), 2306–2320.
- [26] Oscar Koller, Jens Forster, and Hermann Ney. 2015. Continuous sign language recognition: Towards large vocabulary statistical recognition systems handling multiple signers. *Computer vision and image understanding* 141 (2015), 108–125.
- [27] Oscar Koller, Sepehr Zargaran, and Hermann Ney. 2017. Re-sign: Re-aligned end-to-end sequence modelling with deep recurrent CNN-HMMs. In *Proceedings of the IEEE conference on computer vision and pattern recognition*. 4297–4305.
- [28] Dongxu Li, Cristian Rodriguez, Xin Yu, and Hongdong Li. 2020. Word-level deep sign language recognition from video: A new large-scale dataset and methods comparison. In *Proceedings of the IEEE/CVF winter conference on applications of computer vision*. 1459–1469.
- [29] Zecheng Li, Wengang Zhou, Weichao Zhao, Kepeng Wu, Hezhen Hu, and Houqiang Li. 2025. Uni-Sign: Toward Unified Sign Language Understanding at Scale. In *The Thirteenth International Conference on Learning Representations*.
- [30] Jing Lin, Ailing Zeng, Haoqian Wang, Lei Zhang, and Yu Li. 2023. One-stage 3d whole-body mesh recovery with component aware transformer. In *Proceedings of the IEEE/CVF Conference on Computer Vision and Pattern Recognition*. 21159–21168.
- [31] Yuecong Min, Aiming Hao, Xiujuan Chai, and Xilin Chen. 2021. Visual alignment constraint for continuous sign language recognition. In *Proceedings of the IEEE/CVF international conference on computer vision*. 11542–11551.
- [32] Gyeongsik Moon, Shou-I Yu, He Wen, Takaaki Shiratori, and Kyoung Mu Lee. 2020. Interhand2. 6m: A dataset and baseline for 3d interacting hand pose estimation from a single rgb image. In *European Conference on Computer Vision*. Springer, 548–564.
- [33] Priyanka Patel, Chun-Hao P Huang, Joachim Tesch, David T Hoffmann, Shashank Tripathi, and Michael J Black. 2021. AGORA: Avatars in geography optimized for regression analysis. In *Proceedings of the IEEE/CVF Conference on Computer Vision and Pattern Recognition*. 13468–13478.
- [34] Xin Shen, Heming Du, Hongwei Sheng, Shuyun Wang, Hui Chen, Huiqiang Chen, Zhuojie Wu, Xiaobiao Du, Jiaying Ying, Ruihan Lu, et al. 2024. MM-WLAuslan: Multi-Modal Word-Level Australian Sign Language Recognition Dataset. *Advances in Neural Information Processing Systems* 37 (2024), 69700–69715.
- [35] Bowen Shi, Diane Brentari, Gregory Shakhnarovich, and Karen Livescu. 2022. Open-domain sign language translation learned from online video. In *Proceedings of the 2022 Conference on Empirical Methods in Natural Language Processing*. 6365–6379.
- [36] Xingjian Shi, Zhourong Chen, Hao Wang, Dit-Yan Yeung, Wai-Kin Wong, and Wang-chun Woo. 2015. Convolutional LSTM network: A machine learning approach for precipitation nowcasting. *Advances in neural information processing systems* 28 (2015).
- [37] Shengeng Tang, Jiayi He, Dan Guo, Yanyan Wei, Feng Li, and Richang Hong. 2025. Sign-idd: Iconicity disentangled diffusion for sign language production. In *AAAI Conference on Artificial Intelligence*, Vol. 39. 7266–7274.
- [38] Shengeng Tang, Feng Xue, Jingjing Wu, Shuo Wang, and Richang Hong. 2025. Gloss-driven conditional diffusion models for sign language production. *ACM Transactions on Multimedia Computing, Communications and Applications* 21, 4 (2025), 1–17.
- [39] Garrett Tanzer and Biao Zhang. 2024. YouTube-SL-25: A Large-Scale, Open-Domain Multilingual Sign Language Parallel Corpus. *arXiv preprint arXiv:2407.11144* (2024).
- [40] Shuyuan Tu, Zhen Xing, Xintong Han, Zhi-Qi Cheng, Qi Dai, Chong Luo, and Zuxuan Wu. 2025. Stableanimator: High-quality identity-preserving human image animation. In *Proceedings of the Computer Vision and Pattern Recognition Conference*. 21096–21106.
- [41] Dave Uthus, Garrett Tanzer, and Manfred Georg. 2023. Youtube-asl: A large-scale, open-domain american sign language-english parallel corpus. *Advances in Neural Information Processing Systems* 36 (2023), 29029–29047.
- [42] Timo Von Marcard, Roberto Henschel, Michael J Black, Bodo Rosenhahn, and Gerard Pons-Moll. 2018. Recovering accurate 3d human pose in the wild using imus and a moving camera. In *Proceedings of the European conference on computer vision (ECCV)*. 601–617.
- [43] Ching-Chen Wang, Ching-Te Chiu, Chao-Tsung Huang, Yu-Chun Ding, and Li-Wei Wang. 2020. Fast and accurate embedded DCNN for RGB-D based sign language recognition. In *ICASSP 2020-2020 IEEE International Conference on Acoustics, Speech and Signal Processing (ICASSP)*. IEEE, 1568–1572.
- [44] Fei Wang, Kun Li, Yiqi Nie, Zhangling Duan, Peng Zou, Zhiliang Wu, Yuwei Wang, and Yanyan Wei. 2025. Exploiting ensemble learning for cross-view isolated sign language recognition. In *Companion Proceedings of the ACM on Web Conference 2025*. 2453–2457.

- [45] Xu Wang, Shengeng Tang, Peipei Song, Shuo Wang, Dan Guo, and Richang Hong. 2025. Linguistics-vision monotonic consistent network for sign language production. In *ICASSP 2025-2025 IEEE International Conference on Acoustics, Speech and Signal Processing (ICASSP)*. IEEE, 1–5.
- [46] Min Xu, Sheng Liu, Yuan Feng, Yiheng Yu, Zhelun Jin, and Xuhua Yang. 2025. Hierarchical Spatial-Temporal Enhancement Network For Continuous Sign Language Recognition. In *ICASSP 2025-2025 IEEE International Conference on Acoustics, Speech and Signal Processing (ICASSP)*. IEEE, 1–5.
- [47] Yifan Yang, Yuecong Min, and Xilin Chen. 2024. S2net: Skeleton-aware slowfast network for efficient sign language recognition. In *Proceedings of the Asian Conference on Computer Vision*. 319–336.
- [48] Zhendong Yang, Ailing Zeng, Chun Yuan, and Yu Li. 2023. Effective whole-body pose estimation with two-stages distillation. In *Proceedings of the IEEE/CVF International Conference on Computer Vision*. 4210–4220.
- [49] Jiangbin Zheng, Yile Wang, Cheng Tan, Siyuan Li, Ge Wang, Jun Xia, Yidong Chen, and Stan Z Li. 2023. Cvt-slr: Contrastive visual-textual transformation for sign language recognition with variational alignment. In *Proceedings of the IEEE/CVF conference on computer vision and pattern recognition*. 23141–23150.
- [50] Hao Zhou, Wengang Zhou, Weizhen Qi, Junfu Pu, and Houqiang Li. 2021. Improving sign language translation with monolingual data by sign back-translation. In *Proceedings of the IEEE/CVF conference on computer vision and pattern recognition*. 1316–1325.
- [51] Hao Zhou, Wengang Zhou, Yun Zhou, and Houqiang Li. 2020. Spatial-temporal multi-cue network for continuous sign language recognition. In *Proceedings of the AAAI conference on artificial intelligence*, Vol. 34. 13009–13016.
- [52] Ronglai Zuo and Brian Mak. 2022. C2slr: Consistency-enhanced continuous sign language recognition. In *Proceedings of the IEEE/CVF conference on computer vision and pattern recognition*. 5131–5140.